First-Principles Study of High-Pressure Behavior of Solid beta-HMX

ARTICLE *in* THE JOURNAL OF PHYSICAL CHEMISTRY A · DECEMBER 2009

Impact Factor: 2.69 · DOI: 10.1021/jp9090969 · Source: PubMed

7 AUTHORS, INCLUDING:

Dong-Qing Wei
Shanghai Jiao Tong University
225 PUBLICATIONS **4,761** CITATIONS

First-Principles Study of High-Pressure Behavior of Solid β-HMX

Hong-Ling Cui,[†,‡] Guang-Fu Ji,*[,†] Xiang-Rong Chen,[‡,§] Wei-Hua Zhu,[∥] Feng Zhao,[†] Ya Wen,[†] and Dong-Qing Wei[⊥]

National Key Laboratory of Shock Wave and Detonation Physics, Institute of Fluid Physics, Chinese Academy of Engineering Physics, Mianyang 621900, China, Institute of Atomic and Molecular Physics, Sichuan University, Chengdu 610064, China, International Centre for Materials Physics, Chinese Academy of Sciences, Shenyang 110016, China, Institute for Computation in Molecular and Materials Science and Department of Chemistry, Nanjing University of Science and Technology, Nanjing 210094, China, State Key Laboratory of Explosion Science and Technology, Beijing Institute of Technology, Beijing 00081, China

Received: September 21, 2009; Revised Manuscript Received: November 26, 2009

A first-principles plane-wave method with an ultrasoft pseudopotential scheme in the framework of the generalized gradient approximation (GGA) was used to calculate the lattice parameters, bulk modulus and its pressure derivative, energy band structures, density of states, phonon density of states, thermodynamic properties, and absorption spectra of solid β-octahydro-1,3,5,7-tetranitro-1,3,5,7-tetrazocine (β-HMX). The current study is focused on the thermodynamics and electronic properties that were not reported previously. The bulk modulus and its pressure derivative are also consistent with experimental data and other theoretical results. From the results for the band gaps and density of states, it was found that β-HMX has the tendency to become a semiconductor with increasing pressure. As the temperature increases, the heat capacity, enthalpy, product of temperature and entropy, and Debye temperature all increase, whereas the free energy decreases. The optical absorption coefficients shift to higher frequencies/energies with increasing pressure. The present study leads to a better understanding of how energetic materials respond to compression.

1. Introduction

Although highly energetic materials have been used extensively in both civilian and military applications for a long time, their structural, optical, and thermodynamic properties at high pressure are still not well understood. A more detailed investigation of the structure, properties, and stability of these materials under extreme conditions is desired. It is difficult to carry out experiments on the instability of highly energetic materials under high pressure. Furthermore, understanding these properties is very important for the safe, effective, and cost-effective disposal of these materials, because huge stockpiles of highly energetic materials exist at some sites, such as military testing zones, and they contaminate the surrounding land and groundwater.[1−6] Computer simulation is an effective way to comprehend these properties of highly energetic materials at extreme conditions.

HMX (octahydro-1,3,5,7-tetranitro-1,3,5,7-tetrazocine) has been widely used as a secondary explosive since the 1930s. It is also a useful and important component in various high-performance explosives and propellants because of its thermal stability and high detonation velocity.[7,8] HMX is known to exist in four crystalline phases, namely, the three pure crystallization phases α, β, and δ and the hydrated phase γ.[9] The β phase is the most stable form under ambient conditions,[10] whereas α- and δ-HMX are stable at extreme conditions. The β crystalline phase was found to contain two $C_4H_8N_8O_8$ units by X-ray[11] and neutron[12] diffraction (symmetry axis is *b*, 13 independent elastic coefficients). Using synchrotron angle-dispersive X-ray diffraction experiments, Gump et al.[3] obtained isothermal pressure−volume equations of state of β-HMX under temperatures of 303, 373, and 413 K at both hydrostatic and nonhydrostatic compressions. At all of these temperatures, HMX remained in the β phase up to 5.8 GPa. However, at 413 K, upon decompression to ambient from nonhydrostatic pressures above 4 GPa, β-HMX underwent a phase transition to the δ phase.[3] Stevens et al.[4] obtained the complete stiffness tensor of β-HMX by scattering from a variety of acoustic phonons. The observed ordering of stiffness constants is as follows: C_{11} (18.4 GPa) > C_{22} (14.4 GPa) > C_{33} (12.4 GPa).[4] Sewell et al. used a high-level quantum-chemistry-based intramolecular and intermolecular force field to investigate the room-temperature isotherms of the three pure polymorphs of HMX in the pressure range of 0−10.6 GPa and extracted their elastic coefficients and isotropic moduli at room temperature and ambient pressure.[5] Yoo et al. obtained the pressure−volume relations and vibrational Raman spectra of unreacted β-HMX under both quasihydrostatic pressure to 45 GPa and nonhydrostatic pressure to 10 GPa using a diamond-anvil cell, angle-resolved synchrotron X-ray diffraction, and micro-Raman spectroscopy.[13] Their results showed that the high-pressure behavior of β-HMX strongly depends on the stress and that HMX undergoes two phase transitions: a conformational transition at 12 GPa with no apparent abrupt volume change and a discontinuous phase transition at 27 GPa with a volume change.[13] The molecular structures, energetic stabilities, and bulk moduli of the three pure polymorphic forms of crystalline HMX (α, β, δ) were calculated by Lewis et al. using the first-principles electronic-structure method.[14] Henson et al. reported a phase transition from β- to δ-HMX.[15] Furthermore, Xu et al. investigated the structural and optical properties of 3-nitro-1,2,4-triazol-5-one (NTO) crystal using density functional theory.[16] Byrd et al. reported the volume and lattice constants of β-HMX

* Corresponding author. Tel.: +86 816 2485108. E-mail: cyfjkf@caep.ac.cn.
† Chinese Academy of Engineering Physics.
‡ Sichuan University.
§ Chinese Academy of Sciences.
∥ Nanjing University of Science and Technology.
⊥ Beijing Institute of Technology.

10.1021/jp9090969
Published on Web 12/22/2009

up to 8 GPa based on an ab initio study.[17] Zhu et al.[18] reported the electronic and vibrational properties of the four polymorphs of HMX using density functional theory within the local density approximation. The results show that their impact sensitivity order as β-HMX < γ-HMX < α-HMX < δ-HMX.[18] Lu et al. investigated the structural and vibrational properties of β-HMX crystals under hydrostatic pressure using density functional theory with the generalized gradient approximation and found that the N−N bonds were significantly reduced under compression, which might be of importance for initial decomposition.[19] However, to the best of our knowledge the intramolecular geometric structural, electronic, optical, and thermodynamic properties of β-HMX crystals, especially at higher pressure, have not been explored theoretically. Moreover, these properties under pressure are important in better understanding the stability of β-HMX.

In this article, we report calculations of the structure parameters (include the bond lengths, bond angles, and dihedral angles), total energy, density, bulk modulus, energy band gap, density of state, thermodynamic properties, and absorption spectra of β-HMX under different pressures. In section 2, we provide a brief description of our computational method. The results and discussion are presented in section 3, followed by a summary of our conclusions in section 4.

2. Computational Methods

The calculations in this study were performed using density function theory[20] with the Vanderbilt-type ultrasoft pseudopotentials[21] and a plane-wave expansion of the wave functions. The electronic wave functions were obtained using a density-mixing scheme,[22] and the structures were relaxed using the Broyden−Fletcher−Goldfarb−Shannon (BFGS) method.[23] The generalized gradient approximation (GGA)[24] with the Perdew−Burke−Ernzerhof (PBE) parametrization was employed. All calculations were carried out by using the Cambridge Serial Total Energy Package (CASTEP) program.[25] The cutoff energy for plane waves was set to 500.0 eV. The pseudoatomic calculations were performed for H $1s^1$, C $2s^22p^2$, N $2s^22p^3$, and O $2s^22p^4$. Brillouin-zone sampling was performed using the Monkhorst−Pack[26] scheme with a k-point grid of 4 × 2 × 3, which was found to be sufficient for the solid β-HMX with only a weak intermolecular interaction. The values of the kinetic energy cutoff and the k-point grid were determined to ensure the convergence of total energies to within 0.01%. In the geometry relaxation, the total energy of the system converged to less than 1.0×10^{-6} eV/atom, the residual force to less than 0.002 eV/Å, the displacement of atoms to less than 0.002 Å, and the residual bulk stress to less than 0.1 GPa. We adopted the experimental structure[13] a = 6.54 Å, b = 11.05 Å, c = 8.70 Å, and β = 124.3° as the initial structure. Our calculations were conducted on one unit cell with two molecules in the geometry optimization. Starting from the crystal structure of β-HMX optimized at 0 GPa pressure, we applied hydrostatic pressure up to 40 GPa.

3. Results and Discussion

3.1. Crystal Structure at Ambient Pressure. The lattice constants of molecular crystals at ambient pressure provide important information for the crystal structure and a valuable standard for theoretical methods to describe intermolecular interactions at ambient conditions. Figure 1 displays atomic structures of crystalline and molecular β-HMX. The calculated lattice constants and unit-cell volume of β-HMX crystal at ambient pressure are compared with experimental data[13] and

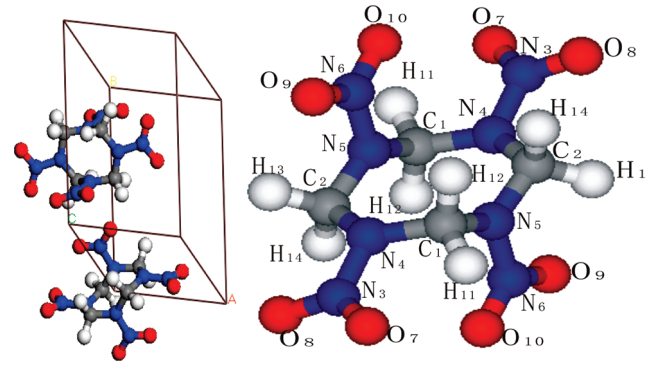

Figure 1. Unit cell of β-HMX crystal (left) and conformation and atomic numbering of $C_4H_8N_8O_8$ molecule in β-HMX (right). Gray, blue, red, and white spheres represent C, N, O, and H atoms, respectively.

TABLE 1: Reported Values of Lattice Constants (Å) and Unit-Cell Volume (Å^3) of Solid β-HMX

	this work	other calculations	experiment[13]
a	6.762	6.78,[a] 6.43,[b] 6.67,[c] 6.57[d]	6.54
b	11.461	11.48,[a] 10.34,[b] 11.17,[c] 11.02[d]	11.05
c	8.865	9.19,[a] 8.61,[b] 8.95,[c] 9.04[d]	8.70
β	123.8	125.02,[a] 124.23,[b] 124.5,[c] 124.9[d]	124.30
V	570.599	585.57,[a] 473.81,[b] 549.30,[c] 531.12[d]	519.39

[a] Reference 19(GGA). [b] Reference 19(LDA). [c] Reference 27 (at 298 K). [d] Reference 28 (at 298 K).

previous theoretical results[19,27,28] in Table 1. Compared with the experimental data,[13] our GGA calculations overestimate a, b, c, β, and V by 3.4%, 3.7%, 1.9%, 0.4%, and 9.9%, respectively. Such differences between theory and experiment are mainly due to a lack of van der Waals (vdW) dispersion forces in the DFT-GGA functional used here. As shown in Table 1, the unit-cell volumes predicted by other theoretical works[27,28] are better than our obtained GGA results. This is mainly because those theoretical works used empirical potentials. Howvever, our calculated volumes agree with previous LDA results.[19]

The intramolecular geometry of β-HMX was calculated using the DFT-GGA function. All bond lengths and bond angles agree with other results.[12,14,19] The average deviations of the calculated bond lengths are about 0.93% for N−N, 1.75% for O−N, 0.576% for N−C, and 1.27% for H−C compared to the experimental data.[12] All bond angles agree with the calculated and experimental results. It is well-known that intramolecular covalent interactions are well-described by DFT with the GGA exchange correlation functional. The good agreement between the GGA results and experiments is reasonable.

3.2. Structure, Total Energy, and Density under High Pressure. We concentrated on β-HMX in the pressure range from 0 to 40 GPa. The crystal structure was relaxed to allow the molecular configurations, cell shape, and volume to change. The obtained pressure−volume relation of β-HMX is shown in Figure 2, together with the results of experiments,[3,13] empirical MD simulations,[5] and other DFT calculations.[19] It is seen that the volume decreases monotonically with increasing pressure. The volume compression is 57.4% up to 40 GPa. In the low-pressure range (0−5 GPa), our results do not adequately predict the volumes. However, the results are in good agreement with the experimental results in the high-pressure range (5−25 GPa). Above 25 GPa, our results are higher than the experiments,[13] which indicates that a phase transition occurred at 27 GPa. Our calculated results indicate that there is no phase transition in this pressure range. Our calculations roughly reproduce the trend

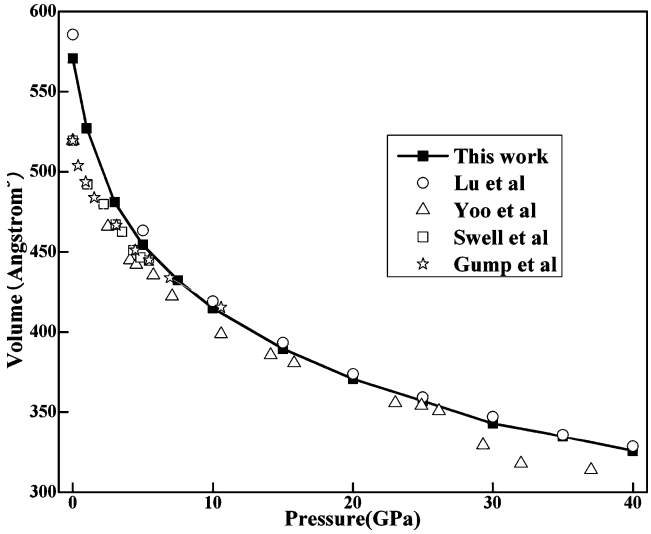

Figure 2. Unit-cell volumes of β-HMX as a function of pressure. The solid squares denote this work. The open stars are from ref 3, the open squares are from ref 5, the open triangles are from ref 13, and the open circles are from ref 19.

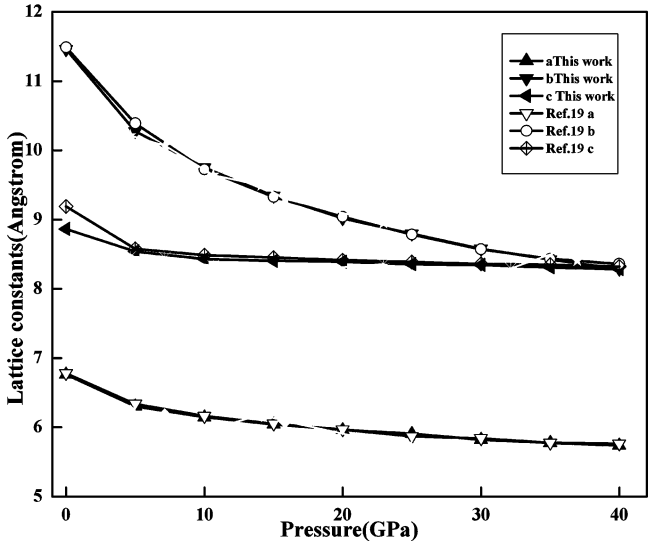

Figure 3. Lattice constants of β-HMX as a function of pressure at 0 K.

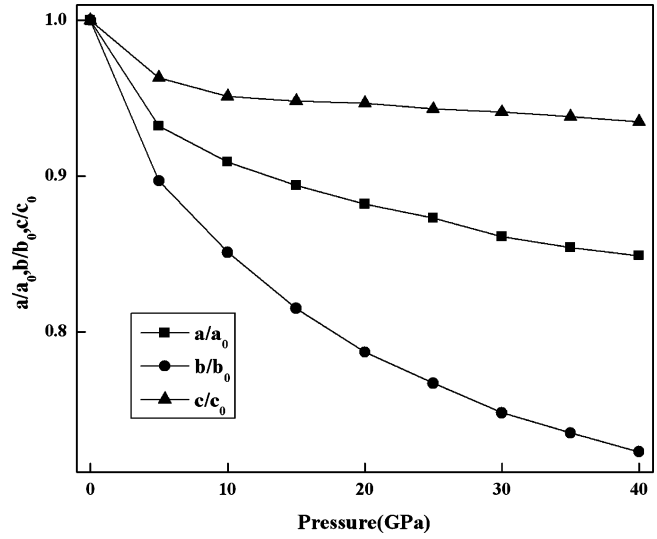

Figure 4. Variation trends with pressure of the ratios a/a_0, b/b_0, and c/c_0 of β-HMX.

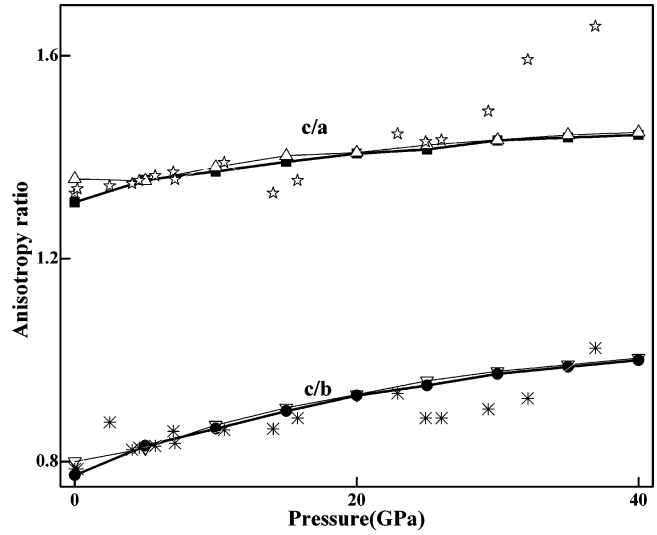

Figure 5. Pressure dependence of the anisotropy ratio for β-HMX at 0 K. The solid lines denote this work, the open dots are from ref 19, and the stars are from ref 13.

of a pressure-induced reduction in volume observed in experiments[3,13] and simulations[5,19] at a given pressure. The dependence of the lattice constants on pressure is shown in Figure 3, along with the experimental data of Yoo et al.[13] and the simulation results of Lu et al.[19] Our calculations overestimate *a*, *b*, and *c* at pressures of less than 5 GPa. The agreement between our calculations and the experiments is rather satisfactory for lattice constants *a*, *b*, and *c* within the range of 5−25 GPa. Above 25 GPa, the calculations overestimate *a* but underestimate *b*. In the pressure range from 0 to 40 GPa, the calculated lattice constants decrease by 15.14%, 27.69%, and 6.54%, respectively. Figure 4 illustrates the trends in the ratios a/a_0, b/b_0, and c/c_0 for β-HMX. It is shown that the *b* axis is the most compressible. In Figure 5, we present the anisotropy ratios *c*/*a* and *c*/*b* with increasing pressure. The *c*/*a* ratio increases from 1.311 at 0 GPa, to 1.355 at 5 GPa, and to 1.415 at 25 GPa, whereas the *c*/*b* ratio increases from 0.773 at 0 GPa, to 0.831 at 5 GPa, and to 0.950 at 25 GPa, which indicates that the compressibility of HMX is anisotropic. This agrees with the results from ref 19.

At the same time, we calculated the bond lengths, bond angles, and dihedral angles of the β-HMX crystal at different pressures. Figure 6 presents the pressure-induced variations of intramolecular bond lengths. Among all types of bonds (i.e., H−C, N−O, N−N, and C−N), the N−N bonds exhibit the most compression, with a maximum variation of 4.92%, which is consistent with the viewpoint that the N−N bond is the weakest bond and might be important in bringing about the initial decomposition reactions of nitramines.[29,30] The C−N bond is also quite compressible. C_2-N_5, C_1-N_4, C_1-N_5, and C_2-N_4 decrease smoothly under compression and are shortened by 4.21%, 3.81%, 3.44%, and 2.47%, respectively. For the four C−H bonds, C_1-H_{11} shows less pronounced reduction, about 1.3% up to 40 GPa, whereas the C_2-H_{14}, C_1-H_{12}, and C_2-H_{13} bond lengths decrease by 1.81%, 1.72%, and 1.45%, respectively. By contrast, the pressure has little effect on the O−N bond lengths. The N_6-O_{10}, N_3-O_7, and N_6-O_9 bonds decrease smoothly by 0.71%, 0.39%, and 1.16%, respectively. However, the N_3-O_8 bond length increases from 0 to 15 GPa but decreases in the range 15−40 GPa and oscillates within 0.3%. This indicates that O−N bonds can be unstable in the β-HMX crystal

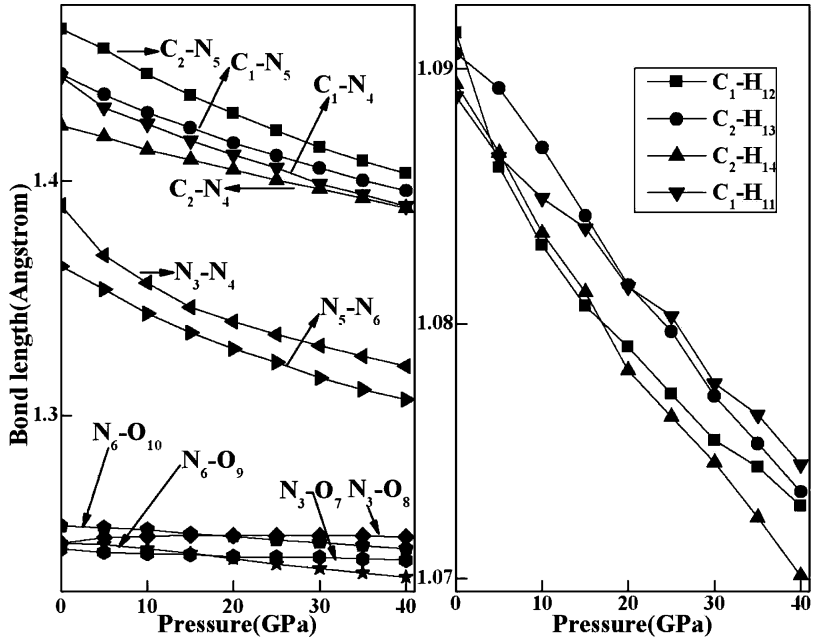

Figure 6. Bond lengths of β-HMX at different pressures.

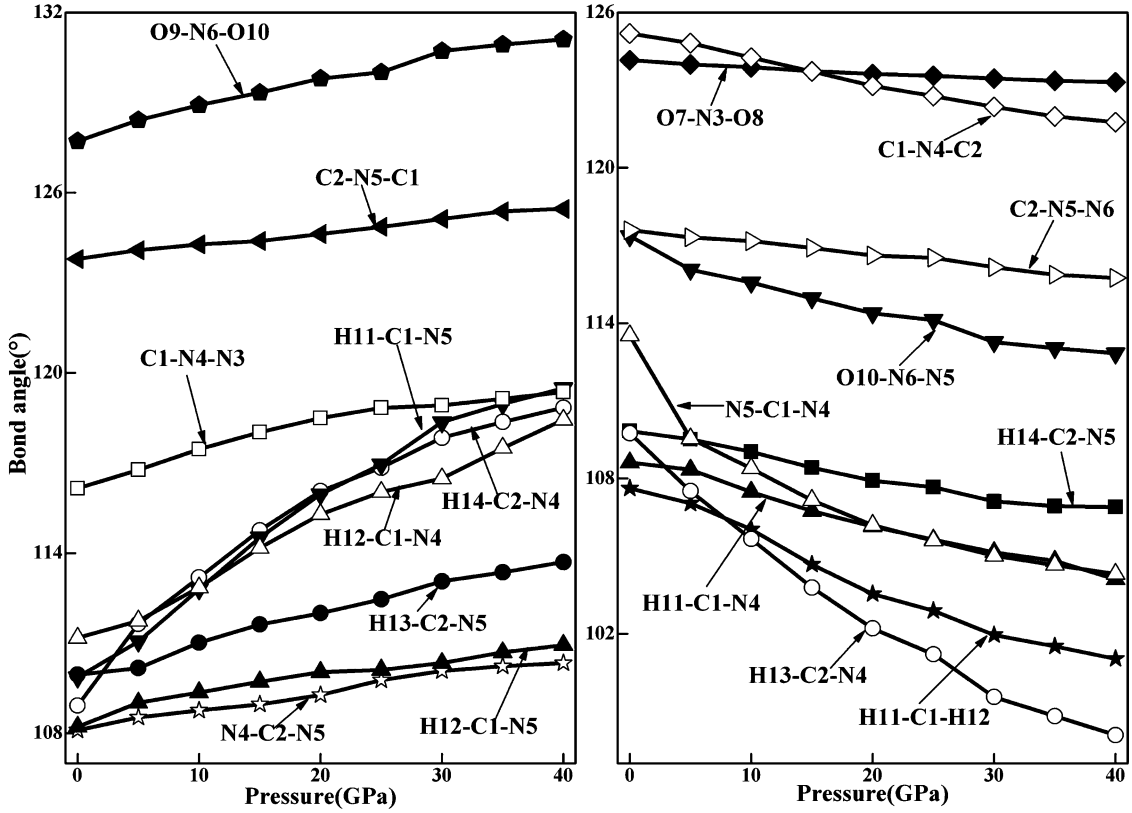

Figure 7. Bond angles of β-HMX at different pressures.

at high pressure. The bond angles and dihedral angles of β-HMX crystal at different pressures are presented in Figures 7−9. From Figure 7, we found that the $C_1-N_4-N_3$, $C_2-N_5-C_1$, $O_9-N_6-O_{10}$, $N_4-C_2-N_5$, $H_{11}-C_1-N_5$, $H_{12}-C_1-N_4$, $H_{12}-C_1-N_5$, $H_{13}-C_2-N_5$, and $H_{14}-C_2-N_4$ bond angles increase with increasing external pressure. The largest percentage increase is for the $H_{14}-C_2-N_4$ bond angle and is 9.11% in the pressure range of 0−40 GPa. The $C_1-N_4-C_2$, $C_2-N_5-N_6$, $O_7-N_3-N_8$, $O_{10}-N_6-N_5$, $N_5-C_1-N_4$, $H_{11}-C_1-N_4$, $H_{11}-C_1-H_{12}$, $H_{13}-C_2-N_4$, and $H_{14}-C_2-N_5$ bond angles decrease with increasing pressure. The largest percentage decrease is 10.62% for the $H_{13}-C_2-N_4$ bond angle from 0 to 40 GPa. The $O_7-N_3-N_4$ bond angle is 116.204° at 0 GPa, and the pressure has little effect on it from 5 to 40 GPa. All of the other bond angles change slightly under compression. The dihedral angles $O_9-N_6-N_5-C_2$ and $N_5-C_2-N_4-C_1$ increase in the pressure from 0 to 5 GPa and decrease from 5 to 40 GPa. From Figure 8, one can see that the dihedral angles $C_1-N_5-C_2-N_4$, $O_7-N_3-N_4-C_1$, $N_4-C_1-N_5-C_2$, $H_{11}-C_1-N_4-N_3$, $H_{11}-C_1-N_5-N_6$, $H_{12}-C_1-N_4-C_2$, $H_{13}-C_2-N_5-N_6$, $H_{14}-C_2-N_4-C_1$, and $H_{14}-C_2-N_5-N_6$ increase with increasing pressure. The greatest percentage change is for the $C_1-N_5-C_2-N_4$ dihedral

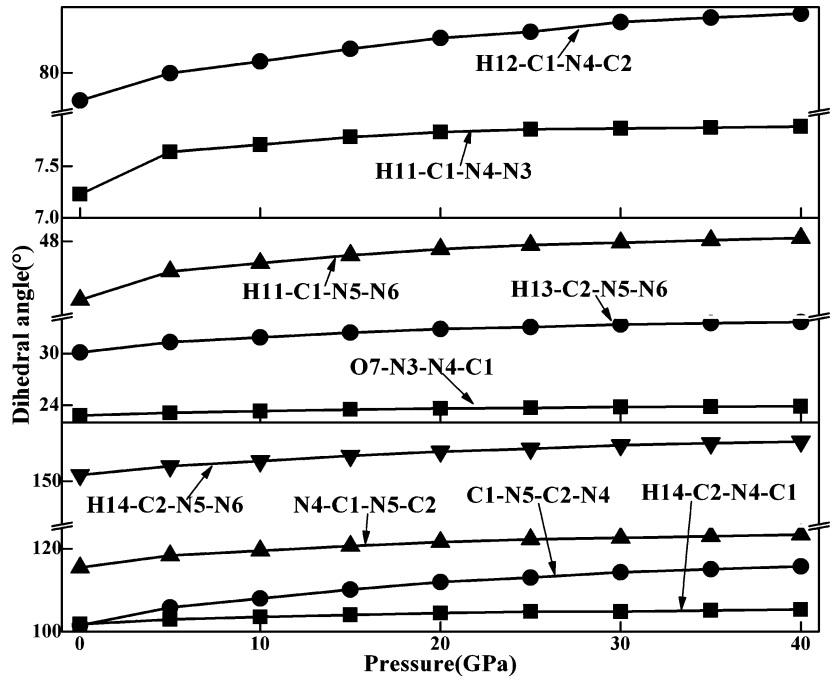

Figure 8. Increasing dihedral angles of β-HMX at different pressures. The *y* axis presents only the numerical value and does not include the direction.

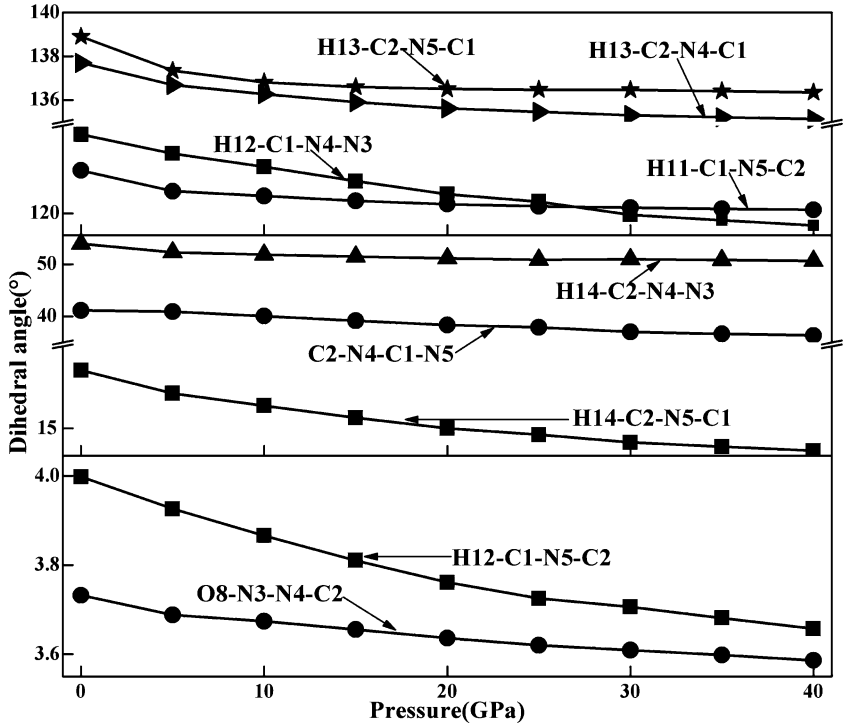

Figure 9. Decreasing dihedral angles of β-HMX at different pressures. The *y* axis presents only the numerical value and does not conclude the direction.

angle and is 14.04%. From Figure 9, we found that the $C_2-N_4-C_1-N_5$, $O_8-N_3-N_4-C_2$, $O_{10}-N_6-N_5-C_1$, $H_{11}-C_1-N_5-C_2$, $H_{12}-C_1-N_4-N_3$, $H_{13}-C_2-N_4-C_1$, $H_{13}-C_2-N_5-C_1$, $H_{14}-C_2-N_5-C_1$, and $H_{14}-C_2-N_4-C_3$ dihedral angles decrease with increasing pressure. The greatest percentage decrease is 17.15% for $H_{14}-C_2-N_5-C_1$. The effects of pressure on all other dihedral angles are very small. These results indicate the primary changes in the ring of the β-HMX crystal under compression. Some of the bond lengths, bond angles, and dihedral angles increase, whereas others decrease. The changes in the bond angles and dihedral angles might result in changes in the intramolecular stress. This, in turn, leads to changes in the energy band and band gap (shown in Figure 12 below) and to an increase in the explosive possibility of β-HMX at high pressure. These changes might be one of the reasons for the initial decomposition reactions of the β-HMX crystal. Therefore, as the pressure increases, the changes in the bond lengths, bond angles, and dihedral angles affect the stability of the β-HMX crystal, especially the changes in the N−N bonds at lower pressures and the changes in the N−O bonds and the $O_7-N_3-N_4$ bond angle at higher pressures. This is because the changes in the bond lengths, bond angles, and dihedral angles

TABLE 2: Comparison of the Bulk Modulus (B_0) of β-HMX and Its First Pressure Derivative (B_0') with Other Studies

	B_0 (GPa)	B_0'
this work	12.5	9.9
Yoo and Cynn[13] (BM[a])	12.4	10.4
Yoo and Cynn[13] (BM[a]) < 12 GPa	16.0	7.3
Lu et al.[19]	6.18	10.4
Sorescu, Rice, and Thompson[28]	14.5	9.6
Olinger, Roof, and Cady[32] (BM[a])	10.6	18.1
Olinger, Roof, and Cady[32] (pv[b]), expt	13.5	9.3

[a] BM = third-order Birch−Murnaghan fitting function, as calculated by Menikoff and Swell. See ref 32. [b] pv = pseudo-velocity fitting function.

might make β-HMX form a "hot spot" easily, thus causing the β-HMX molecule to become unstable.

The total energy and density of β-HMX at different pressures were calculated. The total crystal energy and density increase with increasing pressure. Total energy is lowest at ambient pressure (−12839.07181763 eV) and increases by about 15.11776451 eV up to 40 GPa. The crystal density is 1.72278 g/cm^3 at ambient pressure and over 3.00203 g/cm^3 at about 40 GPa. From the viewpoint of total energy, a β-HMX crystal can be compressed to increase its crystal density.

3.3. Bulk Modulus and Pressure Derivative. We fitted the calculated $E-V$ data to the natural strain equation of state (EOS) developed by Poirier and Tarantola,[31] in which the pressure−volume relationship is expanded to fourth order in strain as

$$P = 3B_0\left(\frac{V_0}{V}\right)f_N\left\{1 + \frac{3}{2}(B' - 2)f_N + \frac{3}{2}[1 + B_0B'' + (B' - 2) + (B' - 2)^2]f_N^2\right\} \quad (1)$$

where $f_N = \ln(l/l_0)$ can be written as $f_N = \ln(V/V_0)/3$ for hydrostatic compression. For truncation at third order in the strain, the implied value of B'' is given by

$$B'' = \frac{-1}{B_0}[1 + (B' - 2) + (B' - 2)^2] \quad (2)$$

We obtained the isothermal bulk modulus B_0 and its pressure derivative B_0' for the β-HMX crystal at $P = 0$ GPa and $T = 0$ K. The results are listed in Table 2, together with other theoretical results and experimental values.[13,19,28,32] Our calculated results agree with other theoretical results[13,28] and with the experimental results.[32] The discrepancies between our results and previous LDA results[19] might be due to different forms used for the equation of state.

3.4. Band Structures and Density of States. The energy bands and density of states (DOS) are important to describe the electronic structures of crystals. The energy band structures and total densities of states for β-HMX at 0 and 25 GPa are presented in Figures 10 and 11, respectively. The Fermi level is taken as the origin of the energy. Both the upper valence bands and the lower conduction bands are flat. From Figure 10, we found that the band gap at 0 GPa is indirect between the G point at the bottom of the conduction bands and the B point at the top of the valence bands. However, the band gap at 25 GPa is direct (G−G), consistent with the direct band gap (G−G) of δ-HMX at 25 GPa. (This shows that there exists a phase transition from β-HMX to δ-HMX crystals, which will be discussed in another work.) The band gaps of β-HMX crystal at different external pressures are displayed in Figure 12. The band gap is 3.47499 eV at 0 GPa, in agreement with the results obtained by Zhu et al.[18] and Lu et al.[19] The band gap is 2.58617 eV at 40 GPa. Moreover, by comparing Figures 10 and 11, one can see that, when the pressure increases, the peaks of the DOS become lower, but the bandwidths become broader, which implies that the electrons become active under compression. The decrease in the energy band gap under compression shows that β-HMX becomes increasingly conductive with increasing pressure, indicating that it might change to a semiconductor or a conductor.

3.5. Phonon Density of States. The partial phonon density of states of β-HMX at 0 GPa is displayed in Figure 13, and the total phonon densities of states at 0 and 25 GPa are shown in Figure 14. By comparing Figures 13 and 14, it can be observed

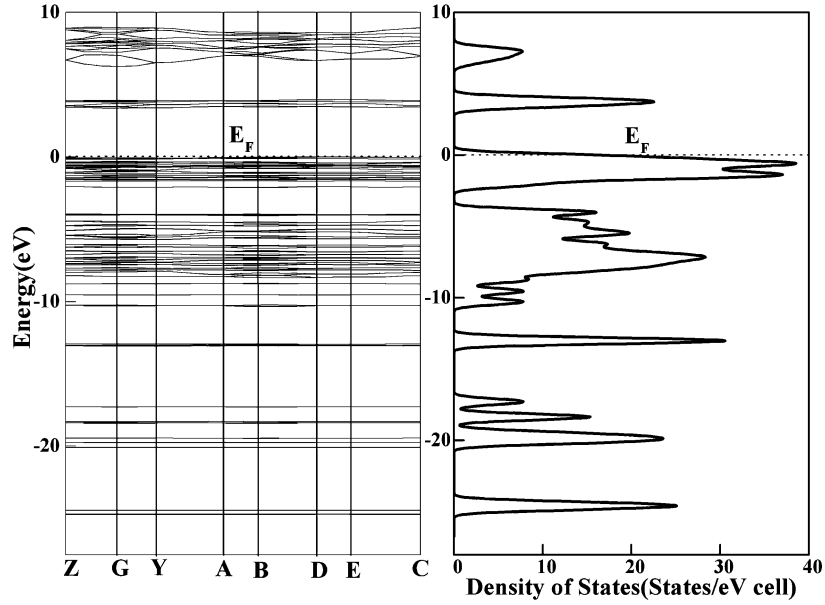

Figure 10. Band structure and total density of states of β-HMX at 0 K and 0 GPa.

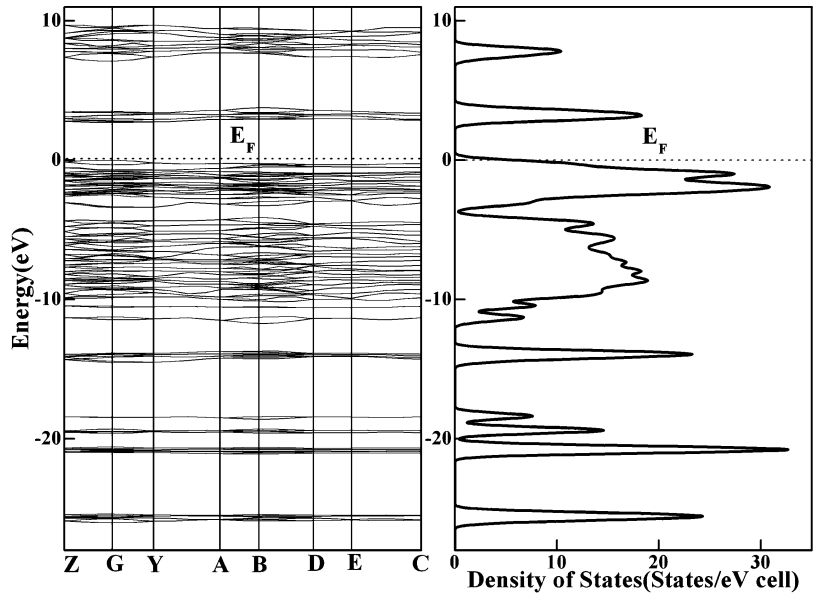

Figure 11. Band structure and total density of states of β-HMX at 0 K and 25 GPa.

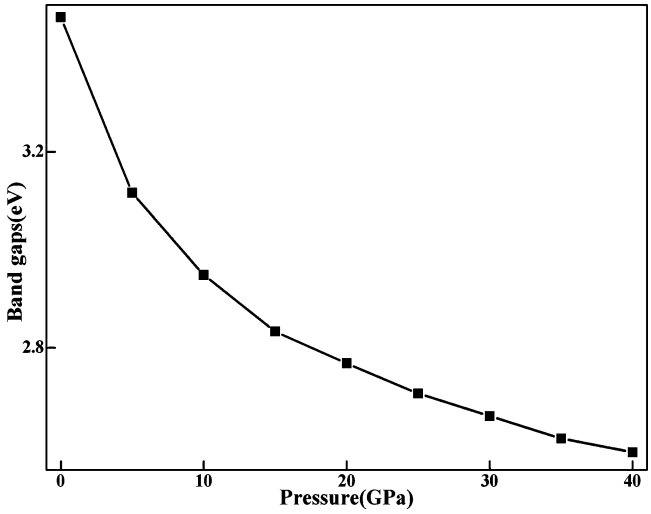

Figure 12. Energy band gaps of β-HMX at 0 K as a function of pressure.

that several sharp peaks at different frequencies originate from C, H, O, and N states. This shows that the C, H, O, and N states play different roles in the phonon DOS. From Figure 13, one can see that the phonon densities of states of C, O, and N in the ring are large in the range 0−44.59 THz, whereas the effects of H states are negligible. The N states of NO_2 make main contributions to the total phonon DOS in the ranges of 18.72−26.13 THz, 27.56−31.74 THz, and 32.43−44.55 THz. The H states play an important role from 32.43 to 44.55 THz and from 63.74 to 65.74 THz. Although the frequency range from 63.74 to 65.74 THz is narrow, the DOS values of H are large in this frequency range. Hence, the H states play a very important role in the frequency range 63.74−65.74 THz. From Figure 14, one can see that the partial phonon DOS makes main contributions to total phonon DOS in the frequency ranges from −3.00 to 44.59 THz at 0 GPa and from −19.22 to 69.32 THz at 25 GPa. However, the values of the phonon density of states of β-HMX are zero in the frequency ranges from 44.62 to 71.36 THz at 0 GPa and from 69.41 to 109.47 THz at 25 GPa. The range of phonon density of states at 25 GPa is clearly widened compared to that at 0 GPa, and there exist large negative frequencies, indicating that the β-HMX crystal is unstable at 25 GPa. From the phonon densities of states of the β-HMX crystal at different pressures, one can conclude that the β-HMX crystal is stable at ambient conditions and becomes more sensitive with increasing pressure, which agrees with the results from ref 10. This is another method for evaluating the stability of the β-HMX crystal at different pressures.

3.6. Thermodynamic Properties. To investigate the thermodynamic properties of β-HMX, two different methods were used. One method is the quasiharmonic Debye model,[33−37] and the other involves the phonon spectra.[38] The free energies, enthalpies, entropies, heat capacities, and Debye temperatures calculated from the quasiharmonic Debye model and phonon spectra are illustrated in Figures 15−17. For simple comparison of the enthalpy results, we present the product of temperature and entropy instead of the entropy. From Figures 15 and 16, it can be seen that the trends in free energy, enthalpy, temperature × entropy, and heat capacity with temperature from two different methods are similar, even though the numerical values exhibit great differences. The enthalpy, temperature × entropy, and heat capacity all increase as the temperature increases, whereas the free energy decreases. However, the calculated Debye temperatures from two methods shown in Figure 17 exhibit a large discrepancy, not only for the numerical values but also for the trend. For the heat capacity, the results from phonon spectra agree with the experimental results.[1] From ref 1, the heat capacity changed from 499.43 to 588.37 J/mol·K in the temperature range from 310 to 440 K. Our calculated heat capacities from phonon spectra vary from 589.97 to 775.93 J/mol·K in the temperature range from 310 to 440 K, whereas those from the quasiharmonic Debye model vary from 1363.59 to 1380.35 J/mol·K in the same temperature range. This discrepancy between the Debye model and the phonon spectra is mainly because the calculations from the Debye model used the quasiharmonic approximation. The quasiharmonic approximation cannot evaluate a system with lower symmetry, such as an organic molecule. Thus, the quasiharmonic Debye model could be inaccurate in the temperature range comparable to the Debye temperature. Consequently, the results from the phonon spectra method are credible. We can estimate the explosion properties of β-HMX crystal from the curve of thermodynamic properties using the phonon spectra method at different temperatures, such as the Hügoniot conditions. The

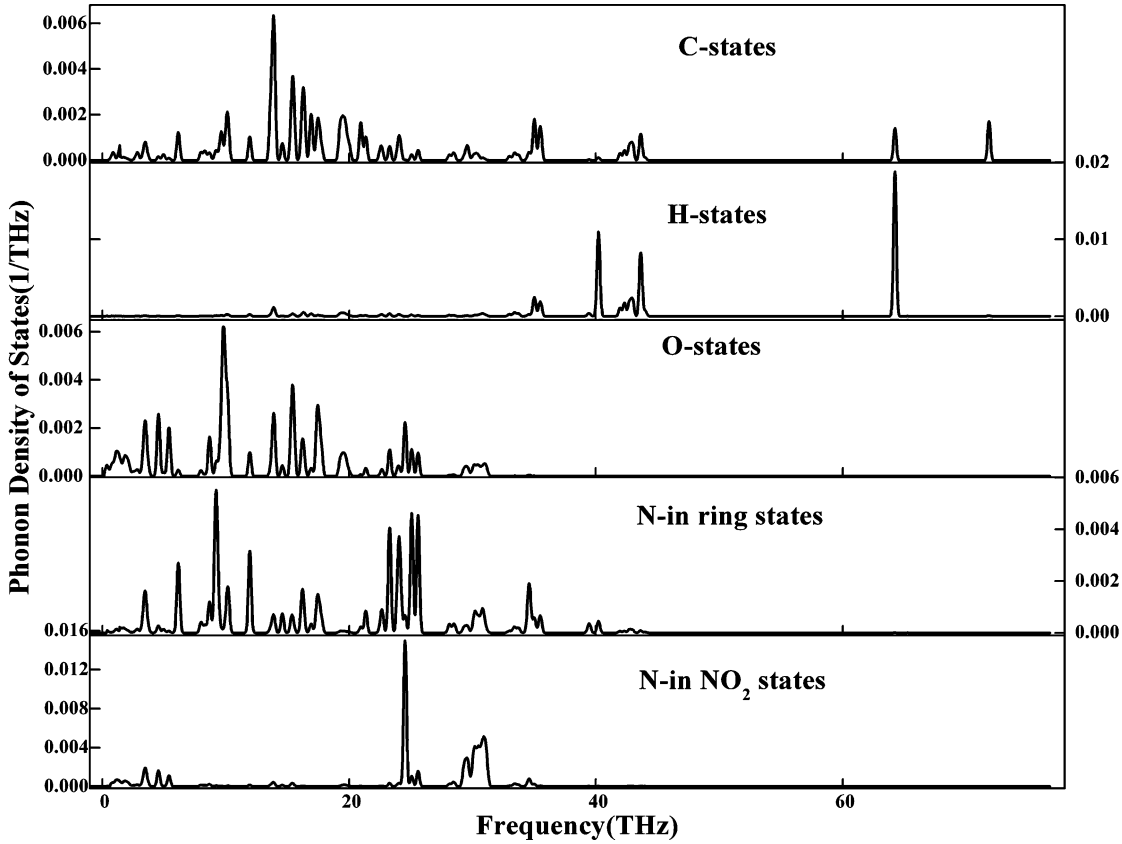

Figure 13. Partial phonon density of states of β-HMX at 0 K and 0 GPa.

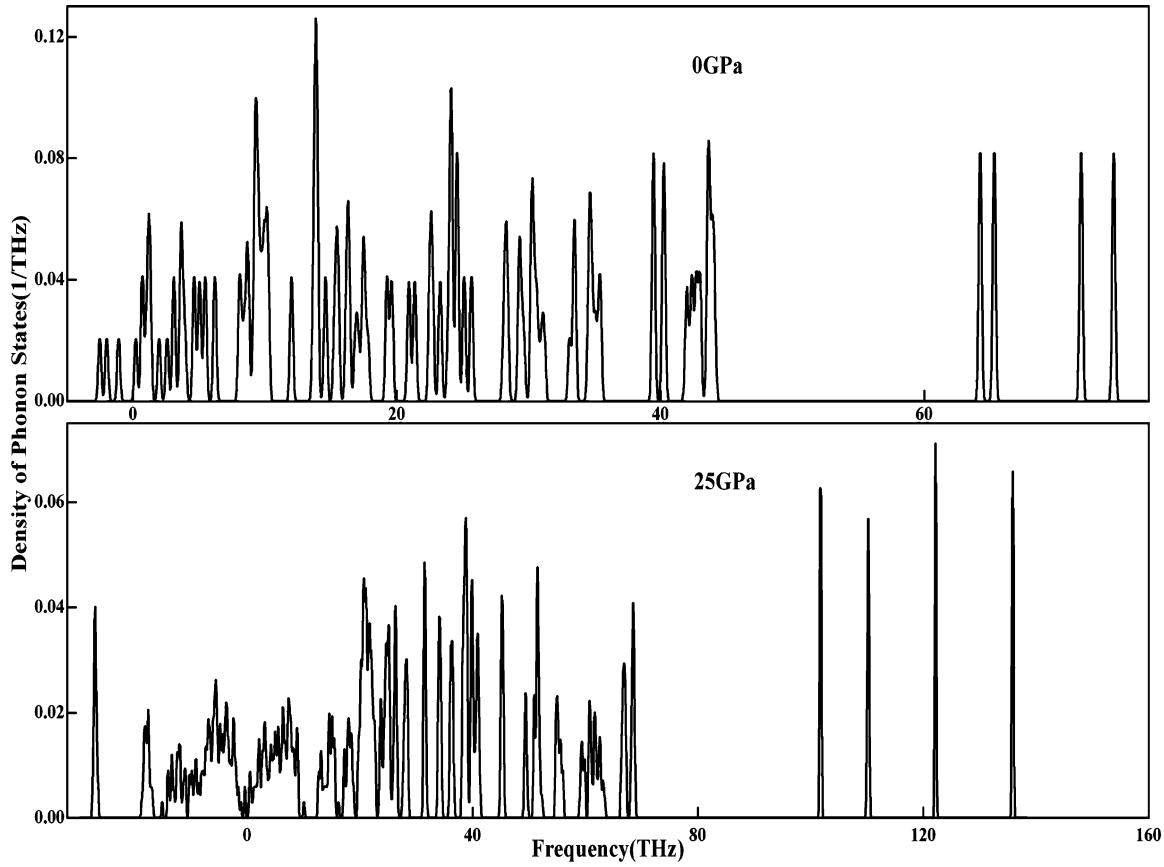

Figure 14. Total phonon density of states of β-HMX at 0 K and 0 and 25 GPa.

variation trends of these thermodynamic properties of the β-HMX crystal will provide hints for experimental research and also be useful for the evaluation of explosive safety under extreme conditions.

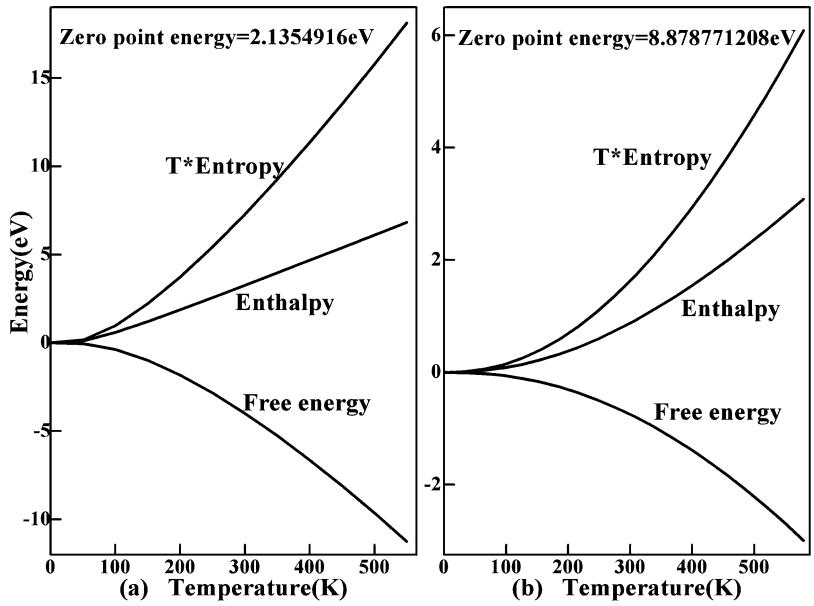

Figure 15. Enthalpy, free energy, and entropy of β-HMX at 0 GPa (a) from the Debye model and (b) from the phonon spectra.

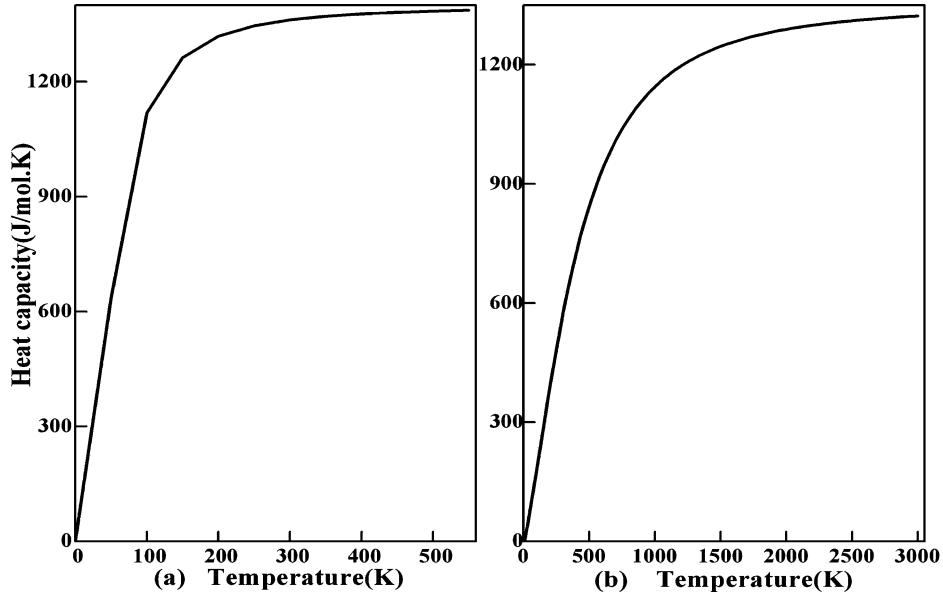

Figure 16. Heat capacity of β-HMX at different temperatures and 0 GPa (a) from the Debye model and (b) from the phonon spectra.

3.7. Absorption Spectra. We also investigated the absorption spectra of β-HMX at different pressures. In this system, the interaction of a photon with electrons can lead to transitions between occupied and unoccupied states. The spectra resulting from these excitations can be depicted as a joint density of states between the valence and conduction bands. The imaginary part of the dielectric function, $\varepsilon_2(\omega)$, can be obtained from the momentum matrix elements between the occupied and unoccupied wave functions based on the selection rules, and the real part of the dielectric function, $\varepsilon_1(\omega)$, can be obtained from the imaginary part by the Kramer−Kronig relationship.[39] The absorption coefficient $\alpha(\omega)$ can be estimated from $\varepsilon_1(\omega)$ and $\varepsilon_2(\omega)$.[39] The absorption coefficients $\alpha(\omega)$ of β-HMX at different external pressures are shown in Figure 18. The first absorption peak in the $\alpha(\omega)$ spectra at ambient pressure is found at 5.73 eV. The absorption coefficient of the band at 5.73 eV was evaluated by our calculations to be 1.267×10^{14} nm^{-1}. At 20 GPa, the magnitude of absorption coefficient $\alpha(\omega)$ of the first absorption peak was found to be 1.518×10^{14} nm^{-1} at 7.48 eV. This shows that an optical transition is allowed. We also found that the first absorption peak at 40 GPa is at 8.03 eV, and the absorption coefficient is 1.513×10^{14} nm^{-1}. Because the absorption coefficient in the fundamental region is high (10^{14} nm^{-1}), β-HMX is unstable and decomposes under the action of light and heat. The absorption peaks of β-HMX at ambient pressure and high pressure are similar but at different energies. In the fundamental absorption region, there are several absorption peaks for β-HMX that are deemed to be related to different exciton states. The absorption peaks of β-HMX increase with increasing pressur,e except that the first absorption peaks decrease. The influence of light on β-HMX becomes more obvious as the pressure increases. Hence, light and heat are both important reasons for the unstability of β-HMX crystals under high pressures. An investigation of the relationship between the absorption spectra and sensitivity for different HMX crystal phases is in progress and will be published elsewhere.

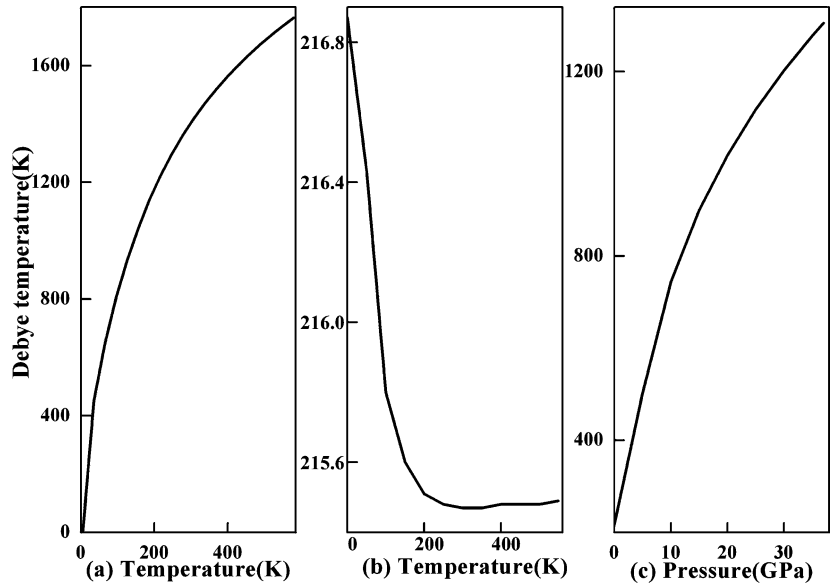

Figure 17. Debye temperature of β-HMX (a) from the phonon spectra and (b) from the Debye model at different temperatures and 0 GPa and (c) from the Debye model at 0 K and different pressures.

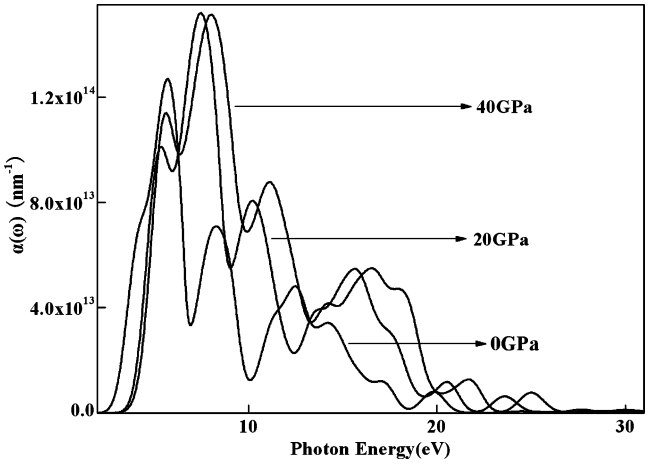

Figure 18. Optical absorption coefficients of β-HMX at high pressure.

4. Conclusions

In this study, we have performed DFT calculations to investigate the lattice parameters, geometries, electronic structures, thermodynamic properties, and absorption spectra of solid β-HMX within the generalized gradient approximation. The results show that the N−N bond lengths of β-HMX rapidly decrease with increasing pressure, but the changes of the N−O bonds lengths and $O_7-N_3-N_4$ bond angle are tiny. Hence, the changes in the N−N bonds are the reason for β-HMX instability at lower pressures, whereas the changes in the N−O bonds and $O_7-N_3-N_4$ bond angle affect the stability of β-HMX at high pressures. The total crystal energy and density increase as the external pressure increases. β-HMX becomes increasingly conductive with increasing pressure, indicating that it might change into a semiconductor or a conductor. The heat capacity, enthalpy, product of temperature and entropy, and Debye temperature all increase with increasing temperature, whereas the free energy decreases. The absorption peaks of β-HMX at low and high pressures are similar. Our calculated bulk modulus and pressure derivative agree with the experimental data and other theoretical results. These are very important properties for understanding the performance of the β-HMX crystal at high pressure.

Acknowledgment. This work was supported by grants from the Shock Wave and Detonation Physics Research of the China Academy of Engineering Physics under Grant 9140C6711010805; the National Science Foundation of China under the Contract 20773085; and the State Key Laboratory of Explosion Science and Technology, Beijing Institute of Technology, under the Contract KFJJ09-2; as well as Rui-Feng Co.; the Virtual Laboratory for Computational Chemistry of CNIC; and the Supercomputing Center of CNIC, Chinese Academy of Sciences.

References and Notes

(1) Gibbs, T. R.; Popolato, A. *LASL Explosive Property Data*; University of California: Berkeley, CA, 1980. Dobratz, B. M. *LLNL Explosives Handbook: Properties of Chemical Explosives and Explosive Simulants*; Report UCRL-52997; Lawrence Livermore National Laboratory: Livermore, CA, 1981.

(2) Zerilli, F. J.; Kuklja, M. M. In *Shock Compression of Condensed Matter, 2007*; Elert, M., Furnish, M. D., Chau, R., Holmes, N., Nguyen, J., Eds.; AIP Conference Proceedings 955; American Institute of Physics: Melville, NY, 2007, p 437.

(3) Gump, J. C.; Peiris, S. M. *J. Appl. Phys.* **2005**, *97*, 053513.

(4) Stevens, L. L.; Eckhardt, C. J. *J. Chem. Phys.* **2005**, *122*, 174701.

(5) Sewell, T. D.; Menikoff, R. *J. Chem. Phys.* **2003**, *119*, 7417.

(6) Lewis, J. P. *Chem. Phys. Lett.* **2003**, *371*, 588.

(7) Cooper, P. W.; Kurowski, S. R. *Introduction to the Technology of Explosives*; Wiley: New York, 1996.

(8) Akhaven, J. *The Chemistry of Explosives*; Royal Society of Chemistry: Cambridge, U.K., 1998.

(9) Cady, H. H.; Smith, L. C. *Studies on the Polymorphs of HMX*; Los Alamos Scientific Laboratory Report LAMS-2652 TID-4500; Los Alamos National Laboratory: Los Alamos, NM, 1961.

(10) Main, P.; Cobbledick, R. E.; Small, R. W. H. *Acta Crystallogr. C* **1985**, *41*, 1351.

(11) Cady, H. H.; Larson, A. C.; Kromer, D. T. *Acta Crystallogr.* **1963**, *16*, 617.

(12) Choi, C. S.; Boutin, H. P. *Acta Crystallogr. B* **1970**, *26*, 1235.

(13) Yoo, C. S.; Cynn, H. *J. Chem. Phys.* **1999**, *111*, 10229.

(14) Lewis, J. P.; Sewell, T. D.; Evans, R. B.; Voth, G. A. *J. Phys. Chem. B* **2000**, *104*, 1009.

(15) Henson, B. F.; Smilowitz, L.; Asay, B. W.; Dickson, P. M. *J. Chem. Phys.* **2002**, *117*, 3780.

(16) Xu, L. N.; Fang, G. Y.; Li, X. H.; Yuan, J. X.; Hu, X. G.; Zhu, W. H.; Xiao, H. M.; Ji, G. F. *J. Mol. Graphics Modell.* **2007**, *26*, 415.

(17) Byrd, E. F. C.; Rice, B. M. *J. Phys. Chem. C* **2007**, *111*, 2787.
(18) Zhu, W. H.; Xiao, J. J.; Ji, G. F.; Zhao, F.; Xiao, H. M. *J. Phys. Chem. B* **2007**, *111*, 12715.
(19) Lu, L. Y.; Wei, D. Q.; Chen, X. R.; Lian, D.; Ji, G. F.; Zhang, Q. M.; Gong, Z. Z. *Mol. Phys.* **2008**, *106*, 2569.
(20) Payne, M. C.; Teter, M. P.; Allan, D. C.; Arias, T. A.; Joannopoulos, J. D. *Rev. Mod. Phys.* **1992**, *64*, 1045.
(21) Vanderbilt, D. *Phys. Rev. B* **1990**, *41*, 7892.
(22) Kresse, G.; Furthmuller, J. *Phys. Rev. B* **1996**, *54*, 11169.
(23) Fischer, T. H.; Almlof, J. *J. Phys. Chem.* **1992**, *96*, 9768.
(24) Perdew, J. P.; Burke, K.; Ernzerhof, M. *Phys. Rev. Lett.* **1996**, *77*, 3865.
(25) Milman, V.; Winkler, B.; White, J. A.; Packard, C. J.; Payne, M. C.; Akhmatskaya, E. V.; Nobes, R. H. *Int. J. Quantum Chem.* **2000**, *77*, 895.
(26) Monkhorst, H. J.; Pack, J. D. *Phys. Rev. B* **1976**, *13*, 5188.
(27) Sewell, T. D. *J. Appl. Phys.* **1998**, *83*, 4142.
(28) Sorescu, D. C.; Rice, B. M.; Thompson, D. L. *J. Phys. Chem. B* **1999**, *103*, 6783.
(29) Brand, H. V.; Rabie, R. L.; Funk, D. J.; Diaz-Acosta, I.; Pulay, P.; Lippert, T. K. *J. Phys. Chem. B* **2002**, *106*, 10594.
(30) Kohno, Y.; Uida, K.; Imamura, A. *J. Phys. Chem.* **1996**, *100*, 4701.
(31) Poirier, J. P.; Tarantola, A. *Phys. Earth Planet. Inter.* **1998**, *109*, 1.
(32) Olinger, B.; Roof, B.; Cady, H. The linear and volume compression of β-HMX and RDX. In *Actes du Symposium International sur le Comportement des Milieux Denses Sous Hautes Pressions Dynamiques*; Commissariat a l'Energie Atomique; Paris, 1978; pp 3−8.
(33) Blanco, M. A.; Francisco, E.; Luana, V. *Comput. Phys. Commun.* **2004**, *158*, 57.
(34) Blanco, M. A.; Martín Pendás, A.; Francisco, E.; Recio, J. M.; Franco, R. *J. Mol. Struct. (THEOCHEM)* **1996**, *368*, 245.
(35) Flórez, M.; Recio, J. M.; Francisco, E.; Blanco, M. A.; Pendás, A. M. *Phy. Rev. B* **2002**, *66*, 144112.
(36) Francisco, E.; Recio, J. M.; Blanco, M. A.; Martín Pendás, A. *J. Phys. Chem. A* **1998**, *102*, 1595.
(37) Francisco, E.; Blanco, M. A.; Sanjurjo, G. *Phys. Rev. B* **2001**, *63*, 094107.
(38) Baroni, S.; Gironcoli, S. de.; Corso Dal, A.; Giannozzi, P. *Rev. Mod. Phys.* **2001**, *73*, 515.
(39) Saha, S.; Sinha, T. P. *Phys. Rev. B* **2000**, *62*, 8828.

JP9090969